A Hybrid Estimation-Based Technique for Partial Discharge Localization

Mohammad Avzayesh, Mamoun F. Abdel-Hafez, *Senior Member, IEEE*, Wasim M. F. Al-Masri, Mohammad AlShabi, *Senior Member, IEEE*, and Ayman H. El-Hag, *Senior Member, IEEE*

***Abstract*— This article demonstrates the use of five different methods to estimate partial discharge (PD) location in an oil insulation system from noisy measurements. The measurements are obtained from three ultrasonic sensors located in three different places. The sensors map the PD location utilizing a nonlinear model. The estimation techniques used in this article are the extended Kalman filter (EKF), the unscented Kalman filter (UKF), the smooth variable structure filter (SVSF), the EK-SVSF, and the UK-SVSF. The last two filters use the combination of EKF or UKF with SVSF, respectively, to consider possible PD model uncertainty. The proposed integrated UK-SVSF algorithm achieves the following objectives. First, the use of the Kaman-based filter enhances the optimality of the filter to system dynamics and measurements noise. Second, the use of the UKF reduces the calculation complexity and errors by replacing the Jacobian calculation with statistical linearization. Finally, the use of the SVSF enhances the estimate's robustness to model uncertainty. The experimental results verify the claim that the PD location estimate with minimum error is achieved by the UK-SVSF.**

***Index Terms*— Acoustic emission sensors, extended Kalman filter (EKF), localization, partial discharge (PD), smooth variable, unscented Kalman filter (UKF).**

I. Introduction

POWER transformers are one of the most critical devices in any power industry and one of the most important components in both distribution and transmission grid. Power transformers' lifetime is greatly related to the health condition of their oil/paper insulation system. Although the aging of their insulation is a natural phenomenon [1], abnormal mechanical, electrical, and thermal stresses cause the aging to be accelerated. This initiates a localized breakdown of the insulation, known as partial discharge (PD) [2], which can lead to the complete failure of the transformer. Therefore, monitoring the PD activities inside power transformers and knowing precisely their locations can increase the life span of these devices.

One of the best approaches to measure the PD is to utilize online measurement techniques. This type of measurement is considered to be a nondestructive monitoring tool for the transformer insulation system. The energy of PD initiation can be transformed into different forms of energy, such as electrical, mechanical, and chemical [2]. Different techniques and sensors can be used to detect the PD activities, such as radio frequency (RF) antenna, high-frequency current transformers (HFCTs), and acoustic emission (AE) sensors [2]. HFCT has a low signal-to-noise ratio. Besides, the ability to use HFCT is influenced by the ability to access the ground wire. Moreover, since only one HFCT is usually used, it cannot be used to localize the PD source unless the winding structure is known. On the other hand, an RF antenna can be used to measure the PD location if multiple antennas are used. However, the use of multiple antennas is intrusive unless they have been preinstalled inside the transformer tank during the manufacturing stage. Moreover, RF antenna has a high sensitivity to electromagnetic pulses, including PD activities. Also, it requires an expensive measuring system as it has a huge bandwidth from hundreds of megahertz to gigahertz.

Conversely, AE measurement systems are relatively cheap as they measure a relatively low-frequency bandwidth (tens to hundreds of kHz). Also, they are nonintrusive as they can be easily installed on the transformer tank using a magnetic holder. However, their performance is affected by the sensor aging, which causes errors in the measurements. Moreover, they are sensitive to external noises, which leads to measurements' errors.

Based on the PD measurement sensor, PD localization methods can be generally divided into two different categories: transfer function and time-of-arrival-based methods. HFCT is used to localize the PD inside a transformer winding precisely, but prior knowledge about the winding transfer function is needed [3]. Such information may not necessarily be available for the field engineer, which limits the application of this approach.

On the other hand, employing either RF antenna [4] or AE sensors [5] does not require any knowledge about the internal structure of the transformer. It is commonly done by estimating the time difference of arrival (TDOA) between the signals captured at multiple sensors attached to the transformer tank. This approach suffers from attenuation due to the different parts of the transformer's internal structure and distortion of the measured signal due to noise.

Manuscript received January 27, 2020; accepted May 26, 2020. Date of publication June 1, 2020; date of current version October 9, 2020. The work was supported in part by the Open Access Program from the American University of Sharjah. This articles represents the opinions of the author(s) and does not mean to represent the position or opinions of the American University of Sharjah. The Associate Editor coordinating the review process was Amitava Chatterjee. *(Corresponding author: Ayman H. El-Hag.)*

Mohammad Avzayesh, Mamoun F. Abdel-Hafez, and Wasim M. F. Al-Masri are with the Department of Mechanical Engineering, American University of Sharjah, Sharjah 26666, UAE.

Mohammad AlShabi is with the Department of Mechanical and Nuclear Engineering, University of Sharjah, Sharjah 27272, UAE.

Ayman H. El-Hag is with the Electrical and Computer Engineering Department, University of Waterloo, Waterloo, ON N2L 3G1, Canada (e-mail: ahalhaj@uwaterloo.ca).

Color versions of one or more of the figures in this article are available online at http://ieeexplore.ieee.org.

Digital Object Identifier 10.1109/TIM.2020.2999165

This work is licensed under a Creative Commons Attribution 4.0 License. For more information, see https://creativecommons.org/licenses/by/4.0/

Ghosh *et al.* [6] utilized the source-filter model to estimate the excitation source and isolate it from the acoustic response of the physical system. Such estimation of the PD pulse can help in determining precisely the TDOA and, hence, the PD location. This approach eliminates the need to use PD denoising techniques. However, the deformation of PD shape could be initiated from sources other than noise, among which are the oil temperature and the obstacles between the PD source and sensor location. Alternatively, a pattern recognition-based method for PD localization in an oil-filled transformer by acoustic measurements was proposed in [7]. The technique is based on splitting the transformer tank into small zones. By comparing the spatial distance between every zone's standard pattern vector and its undetermined pattern vector, the zone with the minimum spatial distance between the two patterns vectors determines the PD location. The accuracy of this model depends on how small are the selected zones. On the other hand, selecting smaller zones will increase the computational complexity.

In this article, the AEs are used to localize the PD inside a transformer insulation system. To obtain an optimal PD estimate that accounts for both the measurement and dynamics noise uncertainty as well as the PD model uncertainty, several estimation techniques are used. The used estimators include the extended Kalman filter (EKF) [8], unscented Kalman filter (UKF) [9], smooth variable structure filter (SVSF) [10]–[12], EK-SVSF [13]–[15], and UK-SVSF [13]–[15]. To the best of the authors' knowledge, UK-SVSF has never been used for nonlinear measurement matrix; previous works defined the system as a nonlinear function and the measurement function as linear or linearized function. The proposed UK-SVSF solves the nonlinearity problem in measurement and system functions without using the Jacobian calculation. The proposed filter achieves the following objectives. First, it produces a solution that targets optimality to measurement and dynamics noise. Second, the filter reduces the calculation and magnitude of the errors by replacing the Jacobian calculations with statistical approximation. Finally, the solution addresses the robustness to model uncertainty through the use of the SVSF.

The rest of this article is organized as follows. Section II is dedicated to the experimental setup, while Section III is dedicated to the methodologies used in this article. Results are discussed in Section IV, and the work is concluded in Section V.

II. Experimental Setup

A high-voltage electrode has been immersed in an oil-filled tank to generate the PD. The electrode is connected to a 40-kV 10-mA 50-/60-Hz ac supply. AE (VS30-SIC-46dB) piezoelectric sensors with a bandwidth range of 20–85 kHz and a resonance frequency of 45 kHz and integrated with 46-dB preamplifier have been used. They are attached to a tank's wall with a magnetic holder. To reduce the reflections on the contact interface, a silicon grease is applied. A digital oscilloscope (TBS 1000) with bandwidth is 60 MHz, and four input channels incorporated with MATLAB is used. The oscilloscope's sampling frequency is set to be 10 million sample/s within a window of 2500 samples. The overall system setup is shown in Figs. 1–3.

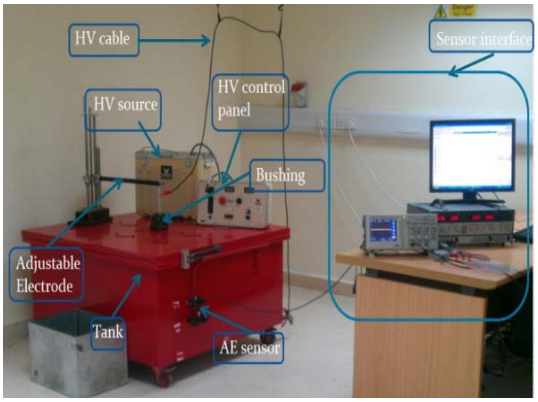

Fig. 1. System setup.

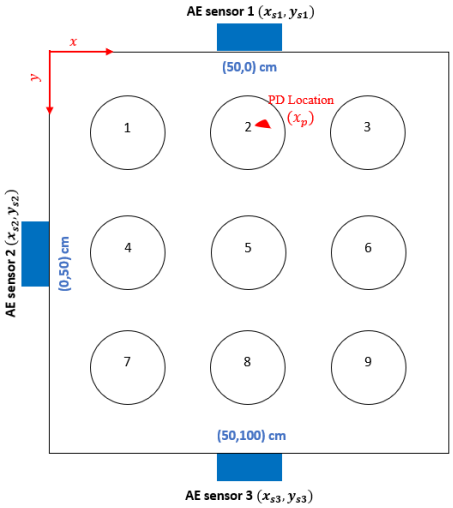

Fig. 2. PD initialization at position 2 without paper insulation barrier.

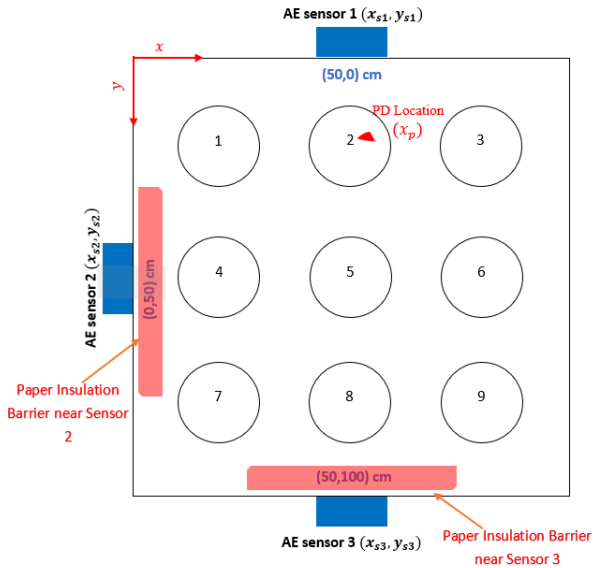

Fig. 3. PD initialization at position 2 with paper insulation barrier.

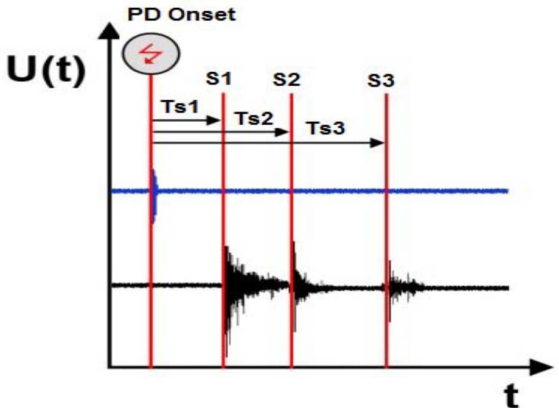

Fig. 4. Schematic drawing of PD initialization to the sensors.

The proposed PD measurement system uses an RF antenna and three AE sensors to measure the distance from each sensor to the PD location, as in (1). As the travel time for an electromagnetic wave is much faster than an acoustic wave, the RF antenna PD measurement is used as a reference for the three AE measurements conducted by the AE sensors. This is shown in Fig. 4, where Ts1, Ts2, and Ts3 are the time difference between the acoustic waves and the RF signal. As in any measurement system, there are two types of propagation errors: systematic and random errors. Our system is mainly concerned with the measurement of the arrival time of different acoustic signals. Bias in the acoustic sensor due to aging and external acoustic noise are two examples of systematic and random errors, respectively, which might influence our time measurement. The tank cover is provided with a different opening to facilitate the application of PD at different locations, as shown in Fig. 2.

To verify the performance of the proposed algorithms to the realistic transformer model, paper insulation barriers were added in front of sensors 2 and 3. The modified transformer's model configuration is shown in Fig. 3. The proposed algorithms' performance with the existence of these barriers will be shown in Section IV. RF antenna has been used to localize the PD in reference to the AE sensors, and the captured signal is shown in Fig. 4.

Knowing the signal transmission time (T_{sa}), the sound velocity (V_s), and the Cartesian sensor i coordinates (x_{si}, y_{si}), the two unknown PD coordinates in space (x, y) can be estimated as in (1); this constitutes a circle's equation

$$(x - x_{\text{si}})^2 + (y - y_{\text{si}})^2 = (V_s T_{\text{si}})^2. \tag{1}$$

The arrangement behind the placement of AE sensors in Fig. 2 has been described in [16] and [17]. The location of PD can be initiated in any area inside one of the nine locations shown in Fig. 2. The measurement equation can be written as in the following equation:

$$z = h(x_p, x_s) + \upsilon + \mu \tag{2}$$

$$h(x_p, x_s) = \begin{bmatrix} \sqrt{(x - x_{s1})^2 + (y - y_{s1})^2} \\ \sqrt{(x - x_{s2})^2 + (y - y_{s2})^2} \\ \sqrt{(x - x_{s3})^2 + (y - y_{s3})^2} \end{bmatrix}. \tag{3}$$

In this equation, z is the sensor measurement, $h(x_p, x_s)$ is the nonlinear relation between PD position and sensors position as described in (3), x_p is the PD's position with the coordinate of (x, y), and x_s is the sensor's position with the coordinate of (x_s, y_s), υ is the vector measurements' noise, and μ is the vector of possible sensors measurements' bias. The model of $h(x_p, x_s)$ is linearized to H around the estimate of the PD position $\bar{x}_p$, as written in (4) and (5). This leads to an error in the measurement Δz, as defined in (6)

$$H = \begin{bmatrix} \frac{\partial h(\bar{x}_p, x_{s1})}{\partial x} & \frac{\partial h(\bar{x}_p, x_{s1})}{\partial y} \\ \frac{\partial h(\bar{x}_p, x_{s2})}{\partial x} & \frac{\partial h(\bar{x}_p, x_{s2})}{\partial y} \\ \frac{\partial h(\bar{x}_p, x_{s3})}{\partial x} & \frac{\partial h(\bar{x}_p, x_{s3})}{\partial y} \end{bmatrix} \tag{4}$$

$$H = \begin{vmatrix} \frac{(\bar{x} - x_{s1})}{\sqrt{(\bar{x} - x_{s1})^2 + (\bar{y} - y_{s1})^2}} & \frac{(\bar{y} - y_{s1})}{\sqrt{(\bar{x} - x_{s1})^2 + (\bar{y} - y_{s1})^2}} \\ \frac{(\bar{x} - x_{s2})}{\sqrt{(\bar{x} - x_{s3})^2 + (\bar{y} - y_{s2})^2}} & \frac{(\bar{y} - y_{s2})}{\sqrt{(\bar{x} - x_{s2})^2 + (\bar{y} - y_{s2})^2}} \\ \frac{(\bar{x}(k+1) - x_{s3})}{\sqrt{(\bar{x} - x_{s3})^2 + (\bar{y} - y_{s3})^2}} & \frac{(\bar{y} - y_{s3})}{\sqrt{(\bar{x} - x_{s3})^2 + (\bar{y} - y_{s3})^2}} \end{vmatrix} \tag{5}$$

$$\Delta z = z - h(\bar{x}_p, x_s) = H \Delta x_p + \upsilon + \mu. \tag{6}$$

III. Methodology

This section describes the filtering techniques used to estimate the PD location from the acquired AE nonlinear measurements.

A. Extended Kalman Filter

The EKF is known as a recursive predictor–corrector filter that fuses the nonlinear measurements to obtain the optimal estimator out of the class of linear estimators [18]. The EKF linearizes the system about the most recent estimates of the state. In doing so, the system's model is linearized to F, which is performed around the most recent *a posteriori* estimate, $\hat{x}_{k|k}$. In addition, the measurement model is linearized to H, which is done around the *a priori* state estimate, $\hat{x}_{k+1|k}$. For the application of Section II, the discretized system and measurement equations are written as follows:

$$x_{k+1} = F x_k + w_k \tag{7}$$

$$z_{k+1} = h(x_{p_{k+1}}, x_s) + \upsilon_{k+1} \tag{8}$$

where $F = I_{2\times 2}$ and z is the measurement after removing the bias term. The EKF formulation is shown in Fig. 5. The dynamic and measurement noise vectors are assumed Gaussian with covariance matrices of Q and R, respectively.

B. Smooth Variable Structure Filter

The variable structure filter (VSF) is another corrector–predictor estimator that was established in 2003. This method uses variable structure theory and sliding mode concept, which steers the gain of the estimator to allow the estimate to converge to the boundary of the true state. This method is not applicable to nonlinear systems [19]. In 2007, the SVSF, a variant of the VSF, was introduced [12]. This method has been established to enhance the robustness of the estimator against model uncertainty and reduce its chattering [11].

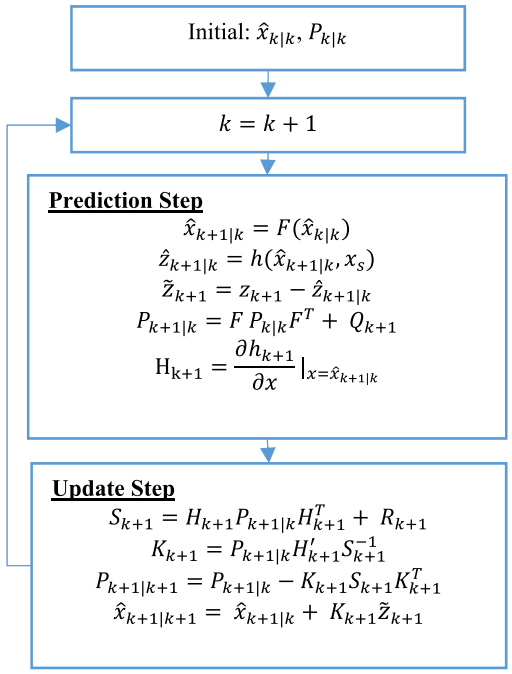

Fig. 5. EXF process.

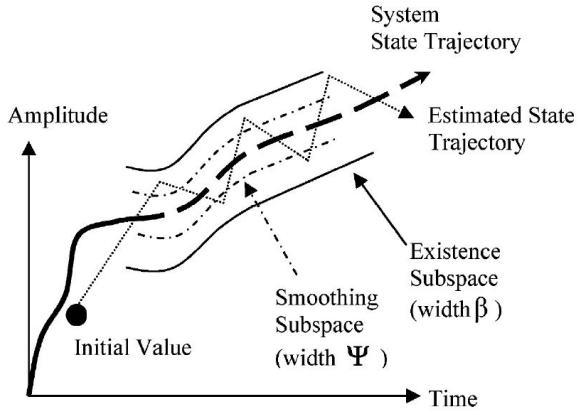

Fig. 6. Chattering effect ($\psi < \beta$) [20].

This is accomplished by using a smoothing boundary layer (SBL) referred to as ψ, forcing a smooth desired trajectory. The existence subspace β denotes the uncertainties in the system. Its width is not known, and it can be assigned based on the design criteria (prior knowledge). If the existence subspace β is greater than the SBL ψ, the chattering occurs, as shown in Fig. 6. The chattering makes the estimator robust. However, the accuracy of the estimate is affected, with a higher estimate's sensitivity to the noise. If the SBL is larger than the existence subspace, the correction gain, as well as the estimator's sensitivity, will be reduced, as shown in Fig. 7. However, the filter's stability will be affected. Therefore, choosing the SBL should be done carefully.

The process of the SVSF is similar to the EKF. However, the gain is calculated as

$$K_{K+1} = H^{+}\mathrm{diag}[\begin{pmatrix}|\tilde{z}_{(k+1|k)}| \\ +\gamma\,|\tilde{z}_{(k|k)}|\end{pmatrix} \circ \mathrm{sat}(\bar{\psi}^{-1}, \tilde{z}_{(k+1|k)})\mathrm{diag}(\tilde{z}_{(k+1|k)})^{-1}] \quad (9)$$

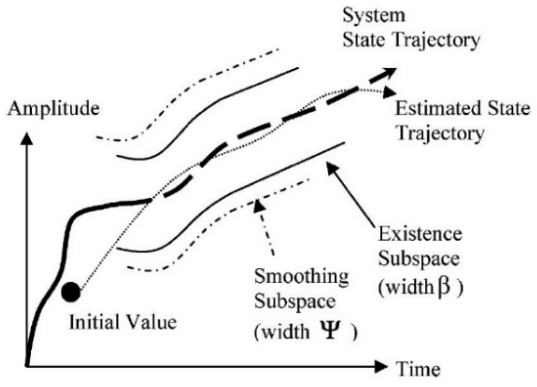

Fig. 7. Smoothed estimation ($\psi > \beta$) [20].

where H^+ is the pseudoinverse of the linearized measurement matrix, $\bar{\psi}$ is the diagonalized SBL, $\tilde{z}_{(k+1|k)}$ and $\tilde{z}_{(k|k)}$ are the innovation error at time k and $k+1$, respectively, and sat is the saturation function, which are represented as

$$\tilde{z}_{(k+1|k)} = z_{(k+1)} - \hat{z}_{(k+1|k)} \quad (10)$$

$$\tilde{z}_{(k|k)} = z_{(k)} - \hat{z}_{(k|k)} \quad (11)$$

$$\mathrm{sat}(\bar{\psi}^{-1}, \tilde{z}_{(k+1|k)}) = \begin{Bmatrix} 1 & \text{if } \frac{\tilde{z}_{(k+1|k)}}{\Psi_{i_{k+1}}} > 1 \\ \frac{\tilde{z}_{(k+1|k)}}{\Psi_{i_{k+1}}} & \text{if } -1 < \frac{\tilde{z}_{(k+1|k)}}{\Psi_{i_{k+1}}} < 1 \\ -1 & \text{if } \frac{\tilde{z}_{(k+1|k)}}{\Psi_{i_{k+1}}} \le -1 \end{Bmatrix}. \quad (12)$$

C. Smoothing Boundary Layer

SBL can be a constant or time-varying vector. In case of a constant SBL, ψ_{constant}, it can be assumed as $n \times n$ diagonal matrix with off-diagonal elements equal to zero and constant diagonal elements found by trial and error as in (12)

$$\psi = \begin{bmatrix} \psi_1 & \cdots & 0 \\ \vdots & \ddots & \vdots \\ 0 & \cdots & \psi_m \end{bmatrix}. \quad (13)$$

For time-varying SBL ψ_{varying}, SBL is the function of the memory or convergence rate γ, the *a priori* and the *a posteriori* errors $\tilde{z}_{(k+1|k)}$ and $\tilde{z}_{(k|k)}$, the linearized measurement matrix H, the *a priori* covariance matrix $P_{(k+1|k)}$, and the innovation covariance matrix $S_{(k+1)}$ as follows [11], [20]

$$\psi^{-1} = \mathrm{diag}(A)^{-1}H\,P_{(k+1||k)}H^T S_{(k+1)}^{-1} \quad (14)$$

$$\psi = \begin{bmatrix} \psi_{11} & \cdots & \psi_{1m} \\ \vdots & \ddots & \vdots \\ \psi_{m1} & \cdots & \psi_{mm} \end{bmatrix} \quad (15)$$

where $\mathrm{A} = (|\tilde{z}_{(k+1|k)}| + \gamma\,|\tilde{z}_{(k|k)}|)$.

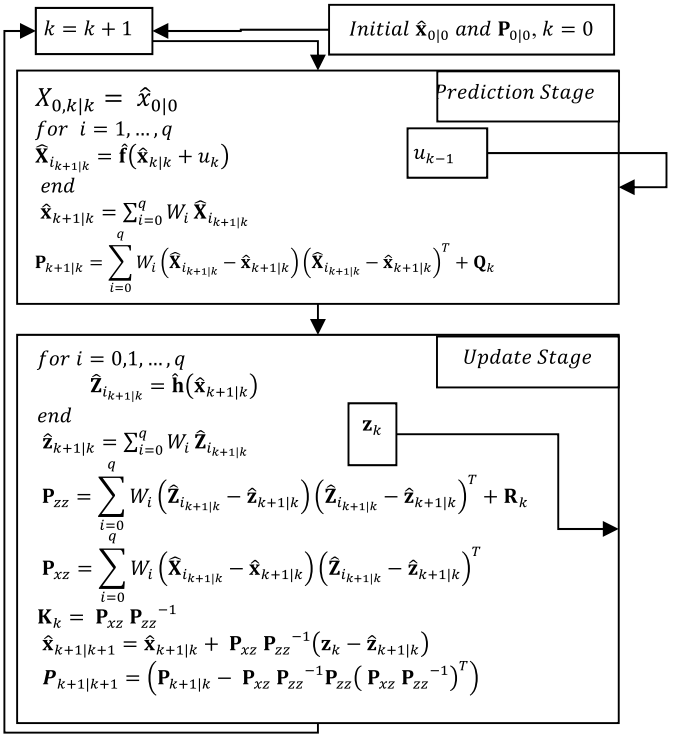

Fig. 8. UKF process [21].

D. Unscented Kalman Filter

The UKF is another extension of KF for nonlinear systems. It replaces the Jacobian calculations by statistical linearization using the unscented transformation [21]. Fig. 8 shows the UKF algorithm. In terms of reliability and accuracy, UKF performs better than EKF. However, it is more complicated in terms of computational cost since it uses $2n + 1$ sigma points to avoid the linearization step of the EKF.

In the prediction stage, $\hat{x}_{k|k-1}$ is the state *a priori* estimate and $\hat{X}_i$ is the sigma point. W_i is the weight factor corresponding to the ith sigma point and can be found as

$$W_i = \frac{1}{2(L + \lambda)} \tag{16}$$

where λ is the design value (usually less than 1) and L is the number of sample points. Then, the *priori* covariance $P_{k|k-1}$ is calculated.

In the update stage, the measurement prediction $\hat{z}_{k+1|k}$ is calculated based on nonlinear propagated measurement $\hat{Z}_{i,k+1|k}$ and the weight corresponds to the ith sample point. The covariance corresponds to measurement prediction $P_{zz,k+1|k}$, and the cross covariance between state estimate and measurement $P_{xz,k+1|k}$ is calculated. In the final step, the *posteriori* state estimate $\hat{x}_{k+1|k+1}$ and its corresponding covariance $P_{k+1|k+1}$ are calculated.

E. EK-SVSF and UK-SVSF

SVSF is proposed to increase the robustness of the filter to modeling uncertainties and, at the same time, enhance the smoothness in the estimated state. However, this comes at the expense of a loss in the estimation accuracy as the SVSF does not optimize the estimated state against dynamics and measurement noise sequences. To obtain a noise-optimal and a model-robust estimator, the SVSF is combined with the EKF and UKF. Two variants of the SVSF, the EK-SVSF, and UK-SVSF, are therefore introduced. The flowchart describing these hybrid filters is shown in Fig. 9 [22].

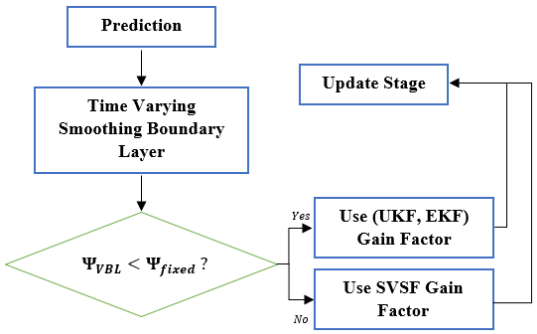

Fig. 9. Combination of different types of KF and SVSF [22].

As can be seen from Fig. 9, after the prediction stage is completed, the variable smoothing boundary layer is calculated based on (14). In addition, a fixed smoothing boundary layer is assigned based on the design criteria. If the fixed boundary layer is greater than the variable smoothing boundary layer, the predicted state is updated based on EKF or UKF. Otherwise, the predicted state is updated based on the SVSF. In the following, we describe the hybrid EKF-SVSF and UK-SVSF formulations.

1) EK-SVSF Formulation: The complete formulation of the EK-SVSF can be summarized as follows. Starting with the current state and its corresponding covariance, $\hat{\mathbf{x}}_{k|k}$ and $P_{k|k}$, respectively, the predicted state, its covariance, and the predicted measurement are obtained as

$$\hat{\mathbf{x}}_{k+1|k} = F(\hat{\mathbf{x}}_{k|k}) \tag{17}$$

$$P_{k+1|k} = \mathrm{F}\mathrm{P}_{k|k}F^T + Q_{k+1} \tag{18}$$

$$\hat{\mathbf{z}}_{k+1|k} = h(\hat{\mathbf{x}}_{k+1|k}, x_s). \tag{19}$$

Subsequently, the innovation error and its covariance are calculated as

$$\tilde{z}_{k+1} = z_{k+1} - \hat{\mathbf{z}}_{k+1|k} \tag{20}$$

$$S_{k+1} = H_{k+1}P_{k+1|}kH_{k+1}^T + R_{k+1}. \tag{21}$$

Then, the variable smoothing boundary layer will be calculated based on

$$\psi_{vbl} = \left(\mathrm{diag}(A)^{-1}H\,P_{k+1|k}H^T S_{k+1}^{-1}\right)^{-1} \tag{22}$$

where $A = \left(\left|\tilde{z}_{(k+1|k)}\right| + \gamma\left|\tilde{z}_{(k|k)}\right|\right)$. The variable smoothing boundary layer is afterward compared against the fixed smoothing boundary layer. If $\Psi_{\text{fixed}} > \Psi_{vbl}$, then the EKF gain factor will be calculated and chosen for state update as

$$K_{k+1} = P_{k+1|k}H_{k+1}^{'}S_{k+1}^{-1}. \tag{23}$$

Otherwise, the SVSF gain factor must be considered for state update as

$$K_{K+1} = H^{+}\mathrm{diag}[\begin{pmatrix} |\tilde{z}_{(k+1|k)}| \\ +\gamma\,|\tilde{z}_{(k|k)}| \end{pmatrix} \circ \mathrm{sat}(\bar{\psi}^{-1}, \tilde{z}_{(k+1|k)})\mathrm{diag}(\tilde{z}_{(k+1|k)})^{-1}]. \quad (24)$$

Then, the state estimate, its covariance, and the measurement estimation will be updated as

$$\hat{\mathbf{x}}_{k+1|k+1} = \hat{\mathbf{x}}_{k+1|k} + K_{k+1}\tilde{z}_{k+1} \quad (25)$$

$$P_{k+1|k+1} = P_{k+1|k} - K_{k+1}S_{k+1}K_{k+1}^{T} \quad (26)$$

$$\hat{\mathbf{z}}_{k+1|k+1} = h(\hat{\mathbf{x}}_{k+1|k+1}, x_s). \quad (27)$$

2) UK-SVSF Formulation: The summarized UK-SVSF formulation can be written as follows. The state estimate, its corresponding, and the sigma point are initialized, as shown in Fig. 8. Then, the sigma points with their corresponding weight are propagated and can be shown as

$$\hat{\mathbf{X}}_{i_{k+1|k}} = \hat{\mathbf{f}}\left(\hat{\mathbf{x}}_{k|k} + u_k\right) \quad (28)$$

$$\hat{\mathbf{x}}_{k|k-1} = \sum_{i=0}^{q} W_i \hat{\mathbf{X}}_{i_{k+1|k}}. \quad (29)$$

The state error covariance can be predicted as

$$\mathbf{P}_{k+1|k} = \sum_{i=0}^{q} W_i \left(\hat{\mathbf{X}}_{i_{k+1|k}} - \hat{\mathbf{x}}_{k+1|k}\right)\left(\hat{\mathbf{X}}_{i_{k+1|k}} - \hat{\mathbf{x}}_{k+1|k}\right)^{T} + \mathbf{Q}_k. \quad (30)$$

In the update stage, the nonlinear measurement is propagated, and the estimated measurement can be calculated as

$$\hat{\mathbf{Z}}_{i_{k+1|k}} = \hat{\mathbf{h}}\left(\hat{\mathbf{x}}_{k+1|k}\right) \quad (31)$$

$$\hat{\mathbf{z}}_{k+1|k} = \sum_{i=0}^{q} W_i \hat{\mathbf{Z}}_{i_{k+1|k}}. \quad (32)$$

The measurement covariance can be calculated as

$$\mathbf{P}_{zz} = \sum_{i=0}^{q} W_i \left(\hat{\mathbf{Z}}_{i_{k+1|k}} - \hat{\mathbf{z}}_{k+1|k}\right)\left(\hat{\mathbf{Z}}_{i_{k+1|k}} - \hat{\mathbf{z}}_{k+1|k}\right)^{T} + \mathbf{R}_k. \quad (33)$$

The cross covariance (between the estimated state and the measurement) is written as

$$\mathbf{P}_{xz} = \sum_{i=0}^{q} W_i \left(\hat{\mathbf{X}}_{i_{k+1|k}} - \hat{\mathbf{x}}_{k+1|k}\right)\left(\hat{\mathbf{Z}}_{i_{k+1|k}} - \hat{\mathbf{z}}_{k+1|k}\right)^{T}. \quad (34)$$

At this stage, similar to the EK-SVSF, the variable smoothing boundary layer is calculated

$$\psi_{\mathrm{vbl}} = \left(\mathrm{diag}(A)^{-1}\mathrm{HP}_{k+1|k}H^{T}S_{k+1}^{-1}\right)^{-1} \quad (35)$$

where $A = \left(|\tilde{z}_{(k+1|k)}| + \gamma\,|\tilde{z}_{(k|k)}|\right)$.

At this stage, the variable smoothing boundary layer is compared with the fixed smoothing boundary layer. If $\Psi_{\mathrm{fixed}} > \Psi_{vbl}$, then the UKF gain factor will be considered and can be calculated as

$$K_k = P_{xz}P_{zz}^{-1} \quad (36)$$

and corresponding estimated state covariance of the UKF is given as

$$P_{k+1|k+1} = \left(P_{k+1|k} - P_{xz}P_{zz}^{-1}P_{zz}\left(P_{xz}P_{zz}^{-1}\right)^{T}\right). \quad (37)$$

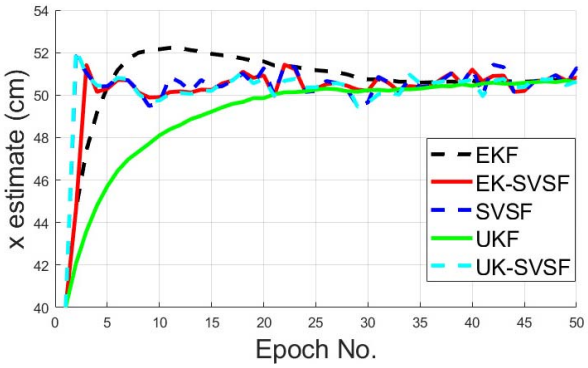

Fig. 10. X-estimate for the first set of measurements without paper insulation barrier.

Otherwise, the SVSF gain factor must be considered

$$K_{K+1} = H^{+}\mathrm{diag}[\begin{pmatrix} |\tilde{z}_{(k+1|k)}| \\ +\gamma\,|\tilde{z}_{(k|k)}| \end{pmatrix} \circ \mathrm{sat}(\bar{\psi}^{-1}, \tilde{z}_{(k+1|k)})\mathrm{diag}(\tilde{z}_{(k+1|k)})^{-1}]. \quad (38)$$

The corresponding covariance of the SVSF state estimate is given as

$$P_{k+1|k+1} = P_{k+1|k} - K_{k+1}S_{k+1}K_{k+1}^{T}. \quad (39)$$

The updated estimate state is then calculated as

$$\hat{\mathbf{x}}_{k+1|k+1} = \hat{\mathbf{x}}_{k+1|k} + K_{k+1}\tilde{z}_{(k+1|k)} \quad (40)$$

where $\tilde{z}_{(k+1|k)} = \mathbf{z}_k - \hat{\mathbf{z}}_{k+1|k}$. The updated estimate of the state is given as

$$\hat{z}_{k+1|k+1} = h(\hat{x}_{k+1|k+1}, x_s). \quad (41)$$

Next, experimental results are shown to validate the performance of the presented algorithms.

IV. Results and Discussion

In this article, four different sets of measurements have been used with 50 measurements in each set. The first data pertains to initiating the PD in location 2 without using a paper insulation barrier, as shown in Fig. 2. The second data set is taken when an insulation paper is introduced in front of sensor 2. The third data set is taken when the insulation paper is introduced in front of sensor 3 (see Fig. 3). Finally, the fourth data set is taken when the position of the PD is changed to position 5 without using the insulation barrier. The EKF, UKF, SVSF, UK-SVSF, and EK-SVSF are used to obtain the estimate of the PD location from the measurements. In the following, the performance of the proposed methods is compared.

A. First Set of Measurement

In this set, 50 measurement points have been used to estimate the PD location. The PD is initialized at position 2, as shown in Fig. 2. The true PD x-coordinate has a value of 50.5 cm, whereas the true PD y-coordinate has a value of 24.5 cm. The results are shown in Figs. 10 and 11 and Table I.

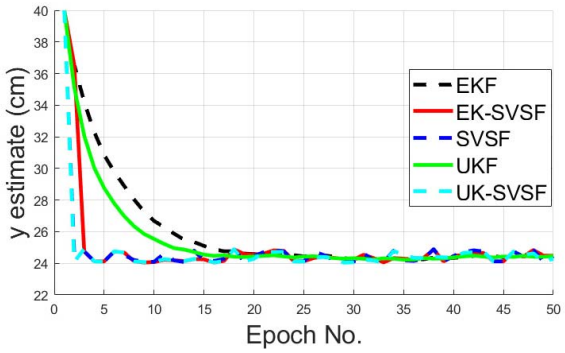

Fig. 11. Y-estimate for the First Set of Measurements without paper insulation barrier.

TABLE I
ROOT MEAN SQUARED ERROR FOR THE FIRST SET OF DATA

	(X-estimate) (cm)	(Y-estimate) (cm)
EKF	0.7823	1.1863
UKF	1.2607	0.3198
SVSF	0.2482	0.0933
EK-SVSF	0.1402	0.0752
UK-SVSF	0.1481	0.0852

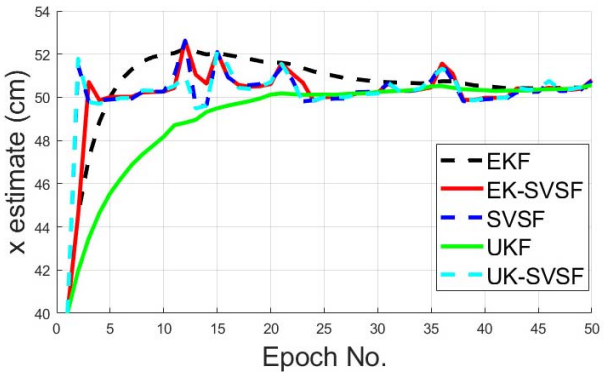

Fig. 12. X-estimate for the second set of measurements with paper insulation barrier near sensor 2.

As can be seen from Figs. 10 and 11, the performances of the EK-SVSF and UK-SVSF are the best among other filters based on the convergence time and the estimation accuracy. Further discussion on these results is given in Section IV-F.

B. Second Set of Measurement

In this set, similar to the first set, 50 measurement points have been used to estimate the PD location, whereas the paper insulation barrier is introduced in front of sensor 2. The PD is initialized at position 2, as shown in Fig. 3. The true PD x-coordinate has a value of 50.5 cm, whereas the true PD y-coordinate has a value of 24.5 cm. The results are shown in Figs. 12 and 13 and Table II.

Figs. 12 and 13 show that the EK-SVSF and UK-SVSF outperform the performance of other filters in terms of estimation accuracy and convergence speed. The detailed explanation is described in Section IV-F.

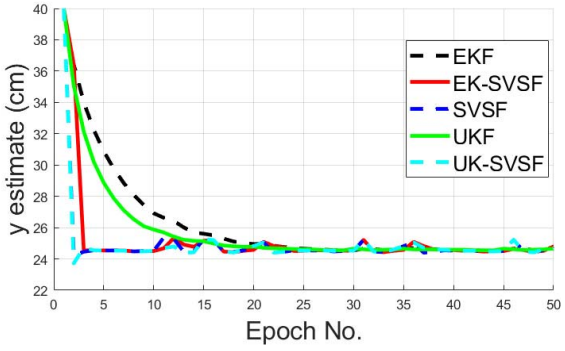

Fig. 13. Y-estimate for the second set of measurements with paper insulation barrier near sensor 2.

TABLE II
ROOT MEAN SQUARED ERROR FOR THE SECOND SET OF DATA

	(X-estimate) (cm)	(Y-estimate) (cm)
EKF	0.7201	1.4240
UKF	1.1549	0.4542
SVSF	0.3714	0.1019
EK-SVSF	0.3251	0.0808
UK-SVSF	0.2783	0.0735

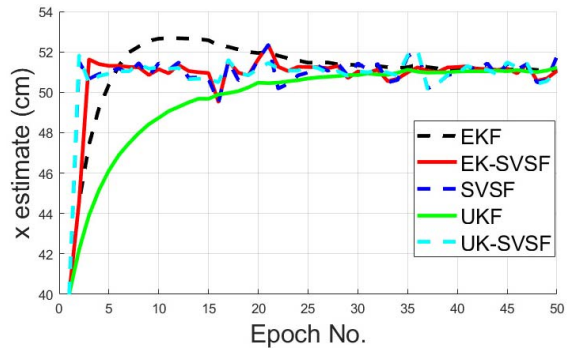

Fig. 14. X-estimate for the third set of measurements with paper insulation barrier near sensor 3.

C. Third Set of Measurement

The third data set is similar to the second data set in terms of the number of measurements, PD initialized location, and the true position in the x-coordinates and y-coordinates. The only difference is the location of the paper insulation barrier, which is placed in front of sensor 3. The results are shown in Figs. 14 and 15 and Table III.

Figs. 14 and 15 show the optimality and robustness of the EK-SVSF and UK-SVSF. Further discussion on the performance of the different filters is given in Section IV-F.

D. Fourth Set of Measurement

The fourth data set is similar to the first three data set in terms of the number of measurements. The PD is initialized at the true position (51, 50.5) in the x-coordinates and y-coordinates, respectively. No insulation paper is added

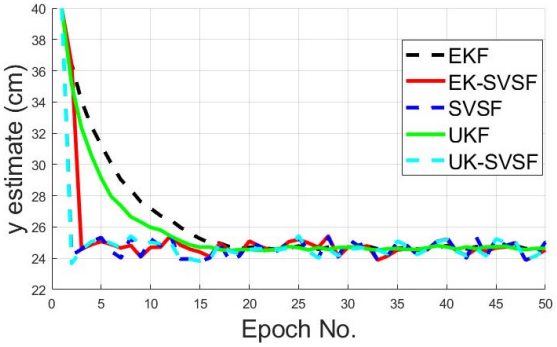

Fig. 15. Y-estimate for the third set of measurements with paper insulation barrier near sensor 3.

TABLE III
ROOT MEAN SQUARED ERROR FOR THE THIRD SET OF DATA

	(X-estimate) (cm)	(Y-estimate) (cm)
EKF	1.6208	1.5176
UKF	0.8150	0.5073
SVSF	0.5676	0.2915
EK-SVSF	0.4797	0.1553
UK-SVSF	0.4310	0.1824

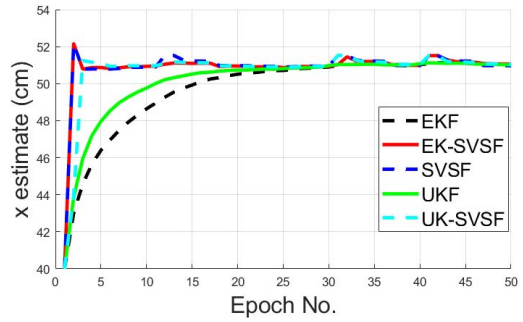

Fig. 16. X-estimate for the fourth set of measurements without paper insulation barrier.

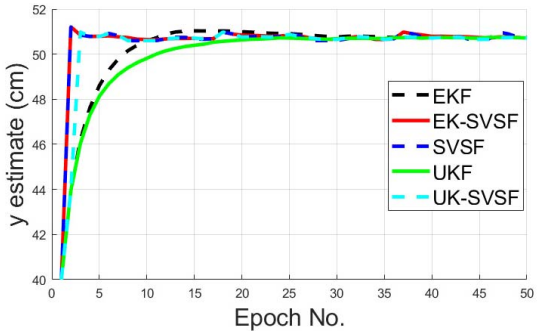

Fig. 17. Y-estimate for the fourth set of measurements without paper insulation barrier.

between the sensor and the barrier. The results are shown in Figs. 16 and 17 and Table IV.

Figs. 16 and 17 show the optimality and robustness of the EK-SVSF and UK-SVSF. Further discussion on the performance of the different filters is given in Section IV-F.

TABLE IV
ROOT MEAN SQUARED ERROR FOR THE FOURTH SET OF DATA

	(X-estimate) (cm)	(Y-estimate) (cm)
EKF	1.1386	0.1308
UKF	0.3261	0.1427
SVSF	0.0535	0.0687
EK-SVSF	0.0289	0.0721
UK-SVSF	0.0350	0.0560

TABLE V
COMPLICATED SCENARIO CONFIGURATION FOR PART D

#	Uncertainties (%)	V_{max}
1	0%	10
2	10%	5
3	20%	1
4	20%	5
5	40%	5

E. Monte Carlo Tests with More Complicated Scenarios of Measurement

The third data set is used again to create more complicated scenarios. These include injecting modeling uncertainties to the coordinates of the sensors with 10%, 20%, and 40% in x and y values, and extra noise to the ultrasonic reading; with maximum absolute value $V_{\max}$ of 1, 5, and 10 cm^2. The noise vector is assumed white with known covariance matrix to be $V_{\max} \times 0.33 \times I_{3\times x}$.

Five scenarios are created with these modeling and noise uncertainties, as listed in Table V. A 10 000 Monte Carlo test was performed on these cases. The root-mean-square error (RMSE) and the maximum absolute error were obtained. The obtained performances of the five scenarios are shown in Tables VI and VII. To enrich the comparison, these methods were compared with the function "fminsearch" from MATLAB that is used to find the solution of the set of equations (1).

F. Discussion

Figs. 10–17 show that all the methods converged to the proximity of the actual value of the PD locations. The filters associated with SVSF show a faster convergence rate compared with EKF and UKF. The combination of EK/UKF with SVSF has improved performance compared with SVSF, which can be seen from the obtained RMSE in Tables I–VII. The tables show that the EK-SVSF and UK-SVSF have the minimum RMSE.

The results of Monte Carlo simulations reported in Tables VI and VII show that the EK-SVSF and UK-SVSF perform sustainably better than all other filters despite the added modeling uncertainty and added measurement noise. The improvement can be seen in both the RMSE and the maximum absolute error. Although increasing the modeling uncertainties reduces the performance of all filters, the UK-SVSF

TABLE VI
MONTE CARLO TESTS, RMSE FOR SCENARIOS WITH INJECTED MODELING UNCERTAINTY AND ADDED MEASUREMENT NOISE

Experiment Number	Root Mean Squared Error											
	EKF		UKF		SVSF		EK-SVSF		UK-SVSF		fminsearch	
	X_Est (cm)	Y_Est (cm)	X_Est (cm)	Y_Est (cm)	X_Est (cm)	Y_Est (cm)	X_Est (cm)	Y_Est (cm)	X_Est (cm)	Y_Est (cm)	X_Est (cm)	Y_Est (cm)
1	0.48	0.80	0.48	0.81	0.53	0.77	0.22	0.74	0.22	0.74	12.5	15.9
2	0.45	0.79	0.45	0.79	0.38	0.74	0.26	0.74	0.26	0.74	8.8	23.2
3	0.41	0.81	0.40	0.81	0.28	0.94	0.31	0.80	0.32	0.80	6.4	17.0
4	2.13	5.40	2.06	5.42	3.22	5.56	0.33	4.32	0.33	4.32	7.3	24.1
5	5.10	12.44	5.03	12.46	5.17	12.79	3.39	9.40	3.39	9.40	7.5	25.7

TABLE VII
MONTE CARLO TESTS, MAXIMUM ABSOLUTE ERROR FOR SCENARIOS WITH INJECTED MODELING UNCERTAINTY AND ADDED MEASUREMENT NOISE

Experiment Number	Maximum Absolute Error											
	EKF		UKF		SVSF		EK-SVSF		UK-SVSF		fminsearch	
	X_Est (cm)	Y_Est (cm)	X_Est (cm)	Y_Est (cm)	X_Est (cm)	Y_Est (cm)	X_Est (cm)	Y_Est (cm)	X_Est (cm)	Y_Est (cm)	X_Est (cm)	Y_Est (cm)
1	1.08	5.50	1.07	5.50	1.48	5.50	0.63	5.50	0.63	5.50	62.7	57.8
2	1.09	5.50	1.08	5.50	1.07	5.50	0.51	5.50	0.51	5.50	29.7	77.3
3	0.96	5.50	0.93	5.50	1.03	5.50	0.6	5.50	0.59	5.50	37.3	71.8
4	3.05	5.97	2.97	5.99	4.83	6.31	0.58	5.50	0.58	5.50	34.2	71.6
5	6.17	13.60	6.10	13.62	7.02	14.2	3.66	10.01	3.66	10.01	44.5	63.0

and the EK-SVSF are much less affected than the EKF, UKF, and SVSF filters. UK-SVSF has slightly better results than the EK-SVSF and is recommended in this study due to its characteristic of avoiding the linearization step of the nonlinear measurement function. The results of using the MATLAB function fminsearch are also included in Tables VI and VII. It is clear that our proposed solution outperforms the results obtained by fminsearch. This is expected as fminsearch only considers the measurements of the sensors. It does not consider possible measurements bias. In addition, it also does not benefit from the dynamic model of the system, as given in (7). Finally, fminsearch does not consider possible model uncertainty.

V. CONCLUSION

PD precise localization is crucial to service engineers as it enables them to identify the PD location and, consequently, its type. Identifying the PD type helps identify the severity of the PD activities. For example, PD in transformer oil is not as significant as PD inside the transformer winding as the earlier could be an indication of merely the existence of air bubbles. However, the later might be an indication of the existence of a transformer winding internal or external discharge. One of the main causes of transformer failure is the existence of PD activities inside the transformer winding.

Five different methods for PD localization were compared in this article: EKF, UKF, SVSF, UK-SVSF, and EK-SVSF. While the EKF and UKF provide an optimal PD estimate in the existence of dynamics and measurement noise sequences, the SVSF provides a PD estimate that considers the possible uncertainty in the dynamics and measurements models. Therefore, in the presented results, the EKF and UKF showed good steady-state error results. However, they converged slowly toward the actual trajectory. Combining the EKF or UKF with SVSF improved the results as the filters converged faster toward the true trajectory, and the estimate's RMSE was the minimum.

In summary, the UK-SVSF method is proposed for PD localization for the following reasons. First, the method produces an estimate that is robust to dynamics and measurements noise sequences. Second, the proposed method reduces the estimation error by utilizing the nonlinear measurement model through the use of the UKF. Finally, the proposed method considers possible model uncertainty through the use of the SVSF structure. Among other factors, the model uncertainty could result from a change in the transformer model due to aging. One of the limitations of this article is the simplistic model of the transformer's internal structure. In the future, the authors will apply the proposed methods in real transformers with full core and windings.

REFERENCES

[1] C.-C. Kuo and H.-L. Shieh, "Artificial classification system of aging period based on insulation status of transformers," in *Proc. Int. Conf. Mach. Learn. Cybern.*, Baoding, China, Jul. 2009, pp. 3310–3315.

[2] J. Rubio-serrano, M. V. Rojas-moreno, J. Posada, J. M. Martínez-tarifa, G. Robles, and J. A. Garcia-souto, "Electro-acoustic detection, identification and location of partial discharge sources in oil-paper insulation systems," *IEEE Trans. Dielectr. Electr. Insul.*, vol. 19, no. 5, pp. 1569–1578, Oct. 2012.

[3] S. Markalous, S. Tenbohlen, and K. Feser, "Detection and location of partial discharges in power transformers using acoustic and electromagnetic signals," *IEEE Trans. Dielectr. Electr. Insul.*, vol. 15, no. 6, pp. 1576–1583, Dec. 2008.
[4] A. Akbari, P. Werle, H. Borsi, and E. Gockenbach, "Transfer function-based partial discharge localization in power transformers: A feasibility study," *IEEE Elect. Insul. Mag.*, vol. 18, no. 5, pp. 22–32, Sep. 2002.
[5] Z. Tang, C. Li, X. Cheng, W. Wang, J. Li, and J. Li, "Partial discharge location in power transformers using wideband RF detection," *IEEE Trans. Dielectr. Electr. Insul.*, vol. 13, no. 6, pp. 1193–1199, Dec. 2006.
[6] R. Ghosh, B. Chatterjee, and S. Dalai, "A method for the localization of partial discharge sources using partial discharge pulse information from acoustic emissions," *IEEE Trans. Dielectr. Electr. Insul.*, vol. 24, no. 1, pp. 237–245, Feb. 2017.
[7] Y. Lu, X. Tan, and X. Hu, "IEE proceedings—Science, measurement and technology," *Inst. Elect. Eng.*, vol. 147, no. 2, pp. 81–85, 2000.
[8] F. Van Der Heidan, R. Duin, D. Ridder, and C. Tax, *Classification, Parameter Estimation and State Estimation—An Engineering Approach Using MATLAB*. Hoboken, NJ, USA: Wiley, 2004.
[9] J. T. Ambadan and Y. Tang, "Sigma-point Kalman filter data assimilation methods for strongly nonlinear systems," *J. Atmos. Sci.*, vol. 66, no. 2, pp. 261–285, Feb. 2009.
[10] M. Al-Shabi, "The general toeplitz/observability smooth variable structure filter," Ph.D. dissertation, McMaster Univ., Hamilton, ON, Canada, 2011. [Online]. Available: http://hdl.handle.net/11375/21180
[11] S. A. Gadsden, "Smooth variable structure filtering: Theory and applications," Ph.D. dissertation, McMaster Univ., Hamilton, ON, Canada, 2011. [Online]. Available: http://hdl.handle.net/11375/11249
[12] S. Habibi, "The smooth variable structure filter," *Proc. IEEE*, vol. 95, no. 5, pp. 1026–1059, May 2007.
[13] S. A. Gadsden and H. H. Afshari, "A review of smooth variable structure filters: Recent advances in theory and applications," *Int. Mech. Eng. Congr. Expo.*, vol. 57397, Nov. 2016, Art. no. V04AT04A055.
[14] H. H. Afshari, S. A. Gadsden, and S. Habibi, "Gaussian filters for parameter and state estimation: A general review of theory and recent trends," *Signal Process.*, vol. 135, pp. 218–238, Jun. 2017.
[15] M. Al-Shabi, S. A. Gadsden, and S. R. Habibi, "Kalman filtering strategies utilizing the chattering effects of the smooth variable structure filter," *Signal Process.*, vol. 93, no. 2, pp. 420–431, Feb. 2013.
[16] W. M. F. Al-Masri, M. F. Abdel-Hafez, and A. H. El-Hag, "A novel bias detection technique for partial discharge localization in oil insulation system," *IEEE Trans. Instrum. Meas.*, vol. 65, no. 2, pp. 448–457, Feb. 2016.
[17] W. M. F. Al-Masri, M. F. Abdel-Hafez, and A. H. El-Hag, "Toward high-accuracy estimation of partial discharge location," *IEEE Trans. Instrum. Meas.*, vol. 65, no. 9, pp. 2145–2153, Sep. 2016.
[18] Y. Bar-Shalom, X.-R. Li, and T. Kirubarajan, *Estimation with Applications to Tracking and Navigation*. New York, NY, USA: Wiley, 2003.
[19] S. R. Habibi and R. Burton, "The variable structure filter," *J. Dyn. Syst. Meas. Control*, vol. 125, no. 3, p. 287, 2003.
[20] S. A. Gadsden and S. Habibi, "An optimal smoothing boundary layer for the smooth variable structure filter," *J. Dyn. Syst.*, vol. 11, p. 1025, Nov. 2011.
[21] R. V. D. Merwe and E. Wan, "The unscented Kalman filter for nonlinear estimation," in *Proc. Adapt. Syst. Signal Process., Commun., Control Symp.*, Oct. 2000, pp. 153–158.
[22] S. A. Gadsden, S. Habibi, and T. Kirubarajan, "Kalman and smooth variable structure filters for robust estimation," *IEEE Trans. Aerosp. Electron. Syst.*, vol. 50, no. 2, pp. 1038–1050, Apr. 2014.

Mohammad Avzayesh received the B.S. degree in mechanical engineering from the University of Sharjah (UAE), Sharjah, UAE, in 2017.

He is currently a Graduate Student in mechanical engineering and a Teaching Assistant with the American University of Sharjah (UAE). His current research interests include state estimation, sensor fusion, and artificial intelligence.

Mamoun F. Abdel-Hafez (Senior Member, IEEE) received the B.S. degree from the Jordan University of Science and Technology, Irbid, Jordan, in 1997, the M.S. degree from the University of Wisconsin, Milwaukee, WI, USA, in 1999, and the Ph.D. degree from the University of California at Los Angeles (UCLA), Los Angeles, CA, USA, in 2003, all in mechanical engineering.

He served as a Post-Doctoral Research Associate with the Department of Mechanical and Aerospace Engineering, UCLA, in 2003, where he was involved in a research project on fault-tolerant autonomous multiple aircraft landing. He is currently a Professor with the Department of Mechanical Engineering, American University of Sharjah, Sharjah, UAE. His research interests include stochastic estimation, control systems, sensor fusion, and fault detection.

Wasim M. F. Al-Masri received the B.S. degree in mechanical engineering (minor) in mechatronics from the Jordan University of Science and Technology, Irbid, Jordan, in 2014, and the M.S. degree in mechatronics engineering from the American University of Sharjah, Sharjah, UAE, in 2016.

He got professional training in King Abdullah II Design and Development Bureau, Amman, Jordan, in 2013. He is currently an Instructor with the Department of Mechanical Engineering, American University of Sharjah, Sharjah, UAE. His current research interests include sensor fusion, state estimation, control theory, robotics, unmanned aerial vehicles, and mechatronics design.

Mohammad AlShabi (Senior Member, IEEE) received the B.Sc. and M.Sc. degrees in mechanical engineering from the Jordan University for Science and Technology, Irbid, Jordan, and the Ph.D. degree in mechanical engineering/mechatronics from McMaster University, Hamilton, ON, Canada, in 2011.

He is currently serving as an Assistant Professor with the Department of Mechanical and Nuclear Engineering, University of Sharjah, Sharjah, UAE. His research areas are control, estimation, robotics, optimization, and artificial intelligence.

Ayman H. El-Hag (Senior Member, IEEE) received the B.S. and M.S. degrees from King Fahd University of Petroleum and Minerals, Dhahran, Saudi Arabia, in 1993 and 1998, respectively, and the Ph.D. degree from the University of Waterloo, Waterloo, ON, Canada, in 2003.

He joined the Saudi Transformer Co., Dammam, Saudi Arabia, as a Quality Control Engineer, from 1993 to 1999. From January 2004 to June 2004, he worked as a Post-Doctoral Fellow with the University of Waterloo. He joined the University of Toronto, Toronto, ON, Canada, as an NSERC Post-Doctoral Fellow, from July 2004 to July 2006. In 2006, he joined the Electrical Engineering Department, American University of Sharjah, Sharjah, UAE. He was promoted to Associate and then to Professor in 2011 and 2016, respectively. He is currently a Lecturer with the Electrical and Computer Engineering Department, University of Waterloo. His current main areas of interest are condition monitoring and diagnostics of electrical insulation and application of machine learning in power engineering.

Dr. El-Hag is a member of the IEEE DEIS Outdoor Insulation Technical Committee and the Co-Founder of the Electric Power and Energy Conversion Systems (EPECS) Conference.